

An ubiquitous mechanism for water-like anomalies

ALAN BARROS DE OLIVEIRA¹, PAULO AUGUSTO NETZ² and MARCIA C. BARBOSA¹

¹ *Universidade Federal do Rio Grande do Sul, Instituto de Física, 91501-970 – Porto Alegre, RS – Brazil*

² *Universidade Federal do Rio Grande do Sul, Instituto de Química, 91501-970 – Porto Alegre, RS – Brazil*

PACS 61.20.Ja – Computer simulation of liquid structure

PACS 61.25.Em – Molecular liquids

PACS 65.20.-w – Thermal properties of liquids

Abstract. - Using collision driven molecular dynamics a system of spherical particles interacting through an effective two length scales potential is studied. The potential can be tuned by means of a single parameter, λ , from a ramp ($\lambda = 0.5$) to a square-shoulder potential ($\lambda = 1.0$) representing a family of two length scales potential in which the shortest interaction distance has higher potential energy than the largest interaction distance. For all the potentials, ranging between the ramp and the square-shoulder, density and structural anomalies were found, while the diffusion anomaly is found in all but in the square-shoulder potential. The presence anomalies in square-shoulder potential, not observed in previous simulations, confirm the assumption that the two length scales potential **is an ubiquitous ingredient for a system to exhibit water-like anomalies.**

Introduction. – Some liquids are known as *anomalous liquids* since they exhibit unexpected behavior upon variations of its thermodynamic conditions. Water is the canonical example of those anomalous liquids.

Water expands upon cooling at fixed pressure [1], diffuses faster upon compression at fixed temperature [2, 3], and becomes less organized upon increasing density – or equivalently upon compression – at constant temperature [4]. These are the density, diffusion, and structural anomalies.

The region where these anomalies occur form nested domes in the density–temperature diagram [4] – or pressure-temperature diagram [5]. The structural anomaly domain occupies the outer region of the pressure-temperature phase-diagram and the density anomaly region is the innermost region. The diffusion anomaly region lies between these two domains [4, 5]. This is the hierarchy of anomalies of water.

Water-like anomalies are also found in other liquids. For example, density anomaly was found experimentally in liquid Te [6], S [7, 8], and $\text{Ge}_{15}\text{Te}_{85}$ [9]. Simulations for silica [10], silicon [11], and liquid beryllium [12] show that density anomaly is also present in these materials. Diffusion and structural anomalies were found for silica [10, 13–15] and silicon [16] and structural anomaly is reported for liquid beryllium [12, 17] through simulations.

In water, the density anomaly is due to the hydro-

gen bonds. The compression of a hydrogen-bonded local environment leads to an increase in entropy, or, equivalently, that a local hydrogen-bonded environment possesses a lower density than a non-bonded system would exhibit [18]. However, there is no hydrogen bond in Te, S and $\text{Ge}_{15}\text{Te}_{85}$.

Therefore, how can the anomalies be explained for bonding and non-bonding systems? In order to address this question, instead of looking for the specific mechanism behind the density anomaly in water or in silica, one has to find the universality behind it.

The simplest framework in which one can look into the physics of anomalies is given by the two length scales potentials. The idea is that in principle an anisotropic interparticle potential can be modeled as effective potential [19]. We will examine one class of effective two length scales potential in which a compression-based competition arises between particles population in the second and first shells.

This assumption was confirmed in a number of isotropic two scales potentials [20–31] in which density, diffusion, and structural anomalies were found. This was also shown to be correct in anisotropic potentials in which the two length scales emerge from the mapping of the anisotropic potential in a equivalent spherical symmetric potential [19, 32]. Ramp-like potentials have demonstrate to be particularly useful since they can describe the effective in-

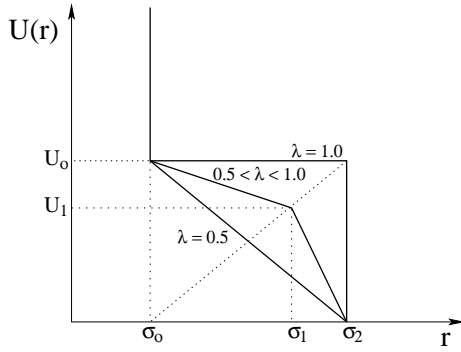


Fig. 1: Interparticle potential studied in this work. The potential can be tuned by means of the parameter λ , ranging from a ramp ($\lambda = 0.5$) to a square-shoulder potential ($\lambda = 1.0$). See the text for more details.

teraction between clusters of water molecules [33, 34]. In fact, Yan *et al.* showed a *quantitative* agreement between the phase-diagram for the ramp potential ($\lambda = 0.5$ in Fig. 1) and that one for the TIP5P molecular model for water [34]. The authors show that a central water molecule interacting with its four nearest neighbors can be modeled effectively through a ramp potential.

A ramp liquid was also used to mimic water in a system composed by a mixture of water and hard-sphere particles [35]. The solvation thermodynamics of the ramp and hard-sphere mixture describes well the qualitative behavior of the water-like solvation thermodynamics [35].

For studying the water-like anomalies the exceptional case is the square-shoulder potential in which no anomalies were reported yet (Fig. 1 with $\lambda = 1.0$) [36]. This led to the idea that anomalies are present in ramp-like potentials (Fig. 1 with $\lambda = 0.5$) but not in shoulder-like potentials.

The aim of this paper is to propose that two scales potentials, potentials in which two preferred distances are present, exhibit water-like anomalies. It will be shown that in some cases the anomalies are in an inaccessible region, as inside a crystal phase. This is the case for the square-shoulder potential [36].

The Model. – In order to test our assumption we developed a tunable potential ranging from a ramp potential to a square-shoulder potential. The potential is given by

$$U(r) = \begin{cases} \infty, & r < \sigma_o \\ \phi_1(r), & \sigma_o < r < \sigma_1 \\ \phi_2(r), & \sigma_1 < r < \sigma_2 \\ 0, & \sigma_2 < r, \end{cases} \quad (1)$$

where $\phi_1(r) = [U_o(\sigma_1 - r) - U_1(\sigma_o - r)] / (\sigma_1 - \sigma_o)$ and $\phi_2(r) = U_1(\sigma_2 - r) / (\sigma_2 - \sigma_1)$.

A single parameter λ is used to tune the potential from a ramp ($\lambda = 0.5$) to a square-shoulder ($\lambda = 1.0$) where $\sigma_1 = \sigma_o + \lambda(\sigma_2 - \sigma_o)$ and $U_1 = \lambda U_o$.

In this work $\sigma_2/\sigma_o = 1.75$ and the potential was approximated by discrete steps in the same spirit of Ref. [37], in such a way that the discrete energy-step is $\Delta U = 0.025U_o$.

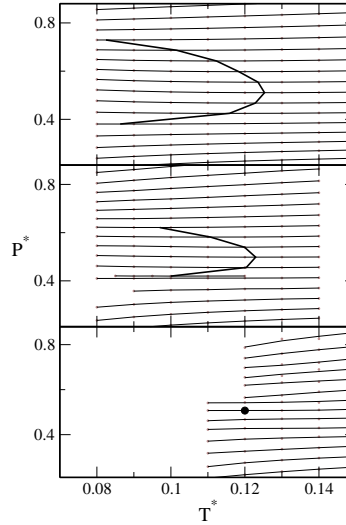


Fig. 2: Pressure-temperature (P-T) diagram for each λ -case. Each line in the P-T diagram corresponds to an isochore: in the upper panel ($\lambda = 0.5$), from bottom to top, they are $\rho^* = 0.20, \dots, 0.34$, and 0.35 . In the middle ($\lambda = 0.6$) isochores are $\rho^* = 0.19, 0.20, 0.21, 0.22, 0.23, 0.232, 0.24, \dots, 0.33$, and 0.34 . Finally, in the lower panel ($\lambda = 1.0$) $\rho^* = 0.17, \dots, 0.29$, and 0.30 . The solid bold line connects the temperature of maximum density (TMD) points and it shrinks to a small region for $\lambda = 1.0$. See the text for details.

Systems with $0.5 \leq \lambda \leq 1.0$ were analyzed for density, diffusion, and structural anomalies.

Using the collision driven molecular dynamics techniques [38], systems with $N = 500$ identical spherical particles of mass m , interacting through the potential Eq. (1) and $\lambda = 0.5, 0.6, 1.0$ were studied. These particles were confined into a cubic box with volume V and periodic boundary conditions. The equilibration and production times were 500 and 1000 respectively, in units of $\sigma_o \sqrt{m/U_o}$ (*time units*). The rescaling of the velocities scheme was used for every 2 time units in order to reach and keep the desired temperature.

Simulations for locating the anomalies at the pressure-temperature phase-diagram were initialized with the system in the fluid phase. This procedure makes possible to sample the metastable liquid phase inside the solid phase.

For estimating the melting line the system was initialized with particles in a face centered cubic configuration. After 500 time units it was checked if the system remains solid or if it has melted. This was done by checking the diffusion coefficient and the shape of the pair distribution function.

This process gave an estimate of the melting line in the pressure-temperature phase-diagram in excellent agreement with the one presented in Ref. [37] for the case in which $\lambda = 0.5$.

Pressure, P , was calculated by means of virial [39] and diffusion, D , was derived from the mean square displacement [39]. The translational order parameter, t , was cal-

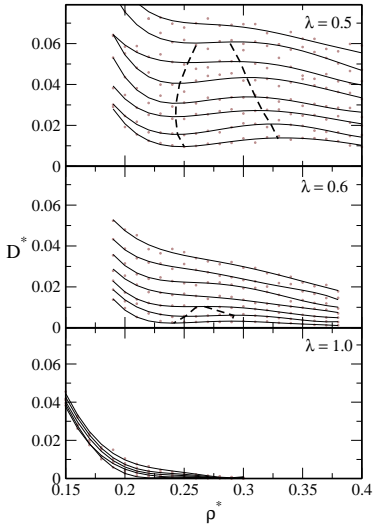


Fig. 3: Diffusion coefficient against density with each line corresponding to an isotherm. Points are simulated data and continuous lines are fifth order polynomial fit from the data. Dashed lines connect maxima and minima in the $D(\rho, T = \text{constant})$ functions and they have the same meaning as in Fig. 6. Between these extrema, diffusion anomalously increases under increasing density – just like water does [2]. In the upper panel ($\lambda = 0.5$ case) the isotherms (from bottom to top) are $T^* = 0.08, 0.09, \dots, 0.14$, and 0.15 . In the middle panel ($\lambda = 0.6$ case) the isotherms are $T^* = 0.08, 0.09, \dots, 0.13$, and 0.14 . Finally, in the lower panel ($\lambda = 1.0$ case), the isotherms are $T^* = 0.11, 0.12, 0.13, 0.14$, and 0.15 .

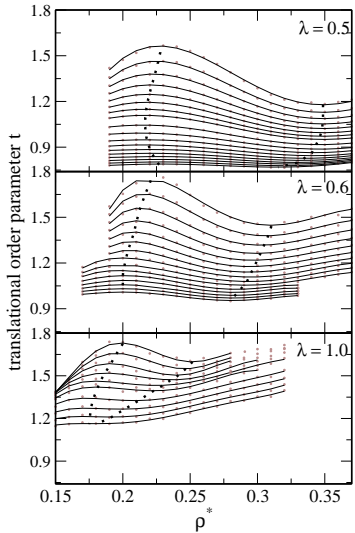


Fig. 4: Translational order parameter, t , versus density for fixed temperatures. Points are simulated data and lines connecting the points are fifth order polynomial fit from the data. Dotted lines bound the region where t decreases under increasing density and they have the same meaning as in Fig. 6. In the upper panel ($\lambda = 0.5$) we show (from top to bottom) the temperatures $T^* = 0.08, 0.09, \dots, 0.14, 0.15, 0.17, 0.19, \dots, 0.33$, and 0.35 . In the middle panel ($\lambda = 0.6$) are shown $T^* = 0.08, 0.09, \dots, 0.21$, and 0.22 . Finally, in the lower panel ($\lambda = 1.0$) temperatures $T^* = 0.11, 0.12, \dots, 0.15, 0.16, 0.18, 0.20, 0.22$, and 0.24 are shown.

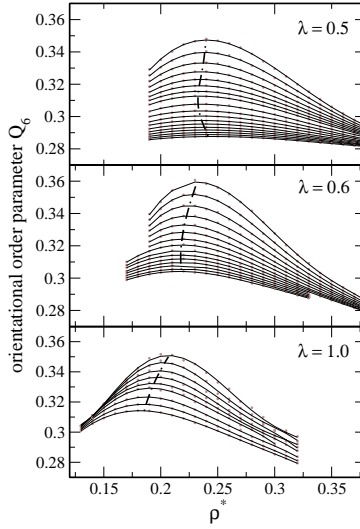


Fig. 5: Orientational order parameter, Q_6 , versus density for fixed temperatures. Points are simulated data and lines connecting the points are fifth order polynomial fit from the data. Dashed-dotted lines connect the maximum values for $Q_6(\rho, T = \text{constant})$ and they have the same meaning as in Fig. 6. The temperatures shown in the three panels are the same as in the Fig. 4.

culated as [4]

$$t \equiv \int_0^{\xi_c} |g(\xi) - 1| d\xi, \quad (2)$$

where $\xi \equiv r\rho^{1/3}$ is the interparticle distance r divided by the mean separation between pairs of particles $\rho^{-1/3}$. $g(\xi)$ is the pair distribution function and ξ_c is a cut-off distance. In this work was used $\xi_c = \rho^{1/3}L/2$, where $L = V^{1/3}$. For a completely uncorrelated system (ideal gas) $g = 1$ and t vanishes. In a crystal, a translational long-order ($g \neq 1$) persists over long distances making t large.

The orientational order parameter [40], Q_6 , was computed using the strategy introduced by Yan *et. al* [29]. Q_6 was calculated as follows. First the spherical harmonics, Y_{lm}^i , associated to each particle i and its k neighbors, were obtained by

$$\langle Y_{lm}^i \rangle = \frac{1}{k} \sum_{j=1}^k Y_{lm}(\theta_{ij}, \phi_{ij}). \quad (3)$$

The $\langle \dots \rangle$ stands for the average over the k neighbors. Details on the calculation of Y_{lm}^i can be found in [21, 29]. The orientational order parameter associated to each particle i is then given by summing the spherical harmonic over all orders m for a fixed degree ℓ namely

$$Q_\ell^i = \left[\frac{4\pi}{2\ell + 1} \sum_{m=-\ell}^{m=\ell} |\langle Y_{lm}^i \rangle|^2 \right]^{1/2}. \quad (4)$$

Then it was chosen $\ell = 6$ for characterizing the local order [21, 29, 32], so the orientational order parameter be-

comes

$$Q_6 = \frac{1}{N} \sum_{i=1}^N Q_6^i, \quad (5)$$

that is the mean value of Q_6^i over all particles of the system.

The parameter Q_6 assumes its maximum value for a perfect crystal and decreases as the system becomes less structured. For a completely uncorrelated system (ideal gas) $Q_6^{ig} = 1/\sqrt{k}$. In this work $k = 12$ neighbors. For a crystal, the Q_6 value depends on the specific crystalline arrangement and on the number of neighbors taken into account.

Pressure, diffusion, temperature, and density, $\rho = N/V$, are given in reduced units as $P^* = P\sigma_o^3/U_o$, $D^* = D(m/U_o)^{1/2}/\sigma_o$, $T^* = k_B T/U_o$, and $\rho^* = \rho\sigma_o^3$.

The Results. – The potentials with $0.5 \leq \lambda \leq 1.0$ were tested for the presence of: a minimum at the isochores in the pressure-temperature phase-diagram; a maximum and a minimum in the diffusion constant as a function of density at constant temperature diagram, a maximum and a minimum in the translational order parameter versus density at constant temperature, and a maximum in the orientational order parameter against density at constant temperature. Then the position of the anomalies were compared with the melting line.

Fig. 2 illustrates the pressure-temperature (P-T) phase-diagram for the potential Eq. (1) with $\lambda = 0.5, 0.6$ and 1.0 . Each line corresponds to an isochores (see the figure caption for details). Some isochores have minima, which define the temperature of maximum density (TMD). For the pressures and the temperatures inside the TMD, the system expands upon cooling under fixed pressure, thus this region is known as the density anomaly region [37]. As λ increases, the density anomaly region shrinks and reduces to a very small region that we identify with a simple point the $\lambda = 1.0$ case. This reduction of the density anomalous region is consistent with simulations for $0.6 < \lambda < 1.0$ (not shown)

Fig. 3 shows the diffusion constant versus density at fixed temperature for $\lambda = 0.5, 0.6$ and 1.0 . For the $\lambda < 0.7$ cases (not shown) the diffusion constant versus density for a fixed temperature has a local maximum and a local minimum (represented by a dashed line in Fig. 3). Between these local extrema the diffusion coefficient increases upon increasing density and this region is known as the diffusion anomaly region.

Figs. 4 and 5 illustrate the translational and the orientational order parameters versus density for constant temperatures for $\lambda = 0.5, 0.6$, and 1.0 . The translational order parameter has a local maximum and a local minimum for an interval of temperatures. Between these local extrema, the parameter t decreases under increasing density. An anomalous t parameter was observed for all λ -cases in the stable liquid phase, even for $\lambda = 1.0$ where no anomalies were reported before. The t anomalous region is bounded

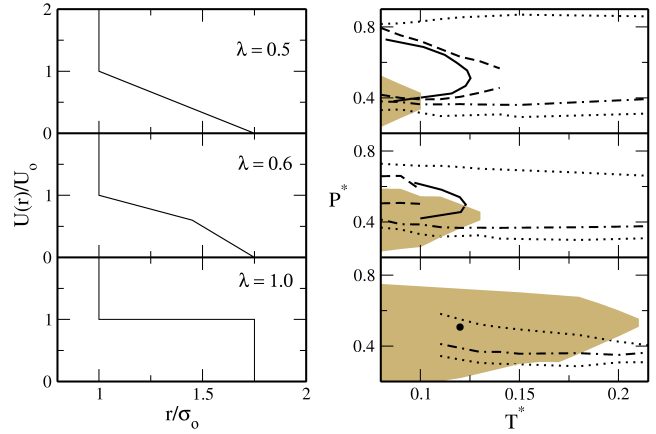


Fig. 6: Interparticle potential studied in this work with $\lambda = 0.5, 0.6$ and 1.0 (left) and the corresponding results we have found (right). Dotted lines enclose the region where t decreases upon increasing density and dashed-dotted line mark the maximum in the Q_6 parameter. The region between the dashed-dotted line and the high pressure dotted line is known as the structural anomaly region (see the text for details). Dashed lines bound the region of diffusion anomaly, and solid line determine the region where density anomaly occurs. For the case with $\lambda = 1.0$ the density anomaly line shrinks into a very small region and the diffusion anomaly region lies inside the solid phase, becoming inaccessible. The shadowed region is bounded by the estimate of the melting line.

by the dotted lines in Fig. 4.

The orientational order parameter, Q_6 , has a maximum in the $Q_6 - \rho$ plane for each isotherm as shown in Fig. 5. For densities higher than the density of maximum Q_6 the orientational order parameter decreases as the density increases – the same trend seen for t .

For each temperature the density of maximum Q_6 lies between between the density of minimum t and the density of maximum t . Consequently for densities between the density of maximum Q_6 and the minimum t is the structural anomaly region. This region is illustrated in Fig. 6.

Fig. 6 summarizes our findings for $\lambda = 0.5, 0.6$, and 1.0 . It shows the regions in the P-T phase-diagram where the density, diffusion, and structural anomalies are located. It also show the location of the melting line that bounds the region where the system becomes solid.

For $\lambda = 0.5$ – the ramp potential case – the high pressure dotted line and the dashed-dotted line bound the region of structural anomalies, where the translational and orientational order parameters decrease with density. A dashed line encloses the diffusion anomaly region where particles diffuse faster upon increasing density. The solid line connects the temperatures of maximum density limiting the density anomaly region. The border of the shadowed region estimates the outer limit for the melting line. For the ramp potential the region of density, diffusion, and structural anomalies are in the stable region of the pres-

sure temperature phase-diagram. All these anomalies for the ramp case are well documented [32, 37] and a further discussion on these results is unnecessary.

For the potentials with $\lambda = 0.6$ and 1.0 shown in Fig. 6 the lines and shadowed region have the same meaning as for the case with $\lambda = 0.5$. Comparing our results for $\lambda = 0.5, 0.6$, and 1.0 an interesting trend is observed. Once the potential become "harder" – going from a ramp to a square-shoulder – three effects are quite evident.

The first effect of the change of λ is related to the mobility of particles in the system. The diffusion anomaly region shrinks as λ increases, moving to lower temperatures becoming inaccessible for the case in which $\lambda = 1.0$. This is in accordance with the results obtained by Netz *et al.* [41]. These authors have observed that as the discretization of the ramp potential becomes less coarser, with corresponding increasing in the energy steps, the diffusion anomaly region shrinks and migrates to lower temperatures into the density anomaly region. Lattice models exhibit this same effect since the lattice structure plays the role of a coarsely discretized energy barriers ambient [42, 43]. In both cases the lines in the pressure temperature phase-diagram defining the border between the density and diffusion anomalous regions cross for a certain choice of parameters what is also observed for $\lambda = 0.6$.

The second effect is related to the melting line. As λ increases the estimate of the melting line goes towards high temperatures, engulfing the region of water-like anomalies. This could explain why no anomalies were reported for the case with $\lambda = 1.0$.

The third effect is related to both the structural and density anomaly regions. As λ increases the temperature of these regions are not drastically affected. This is consistent with the results obtained by Netz *et al.* [41], where the authors have observed that the discretization of the ramp potential does not affect the thermodynamics. In the current case, as λ increases the potential not only becomes more discretized but also there is a change in the potential energy associated with each scale. This leads to a shrink in the pressure range of the anomalous region.

We can also gain some insight on the relationship between structure of the system, shape of the effective interparticle potential, and presence of anomalies by analyzing the order map, i.e., the $t - Q_6$ plane [4, 21, 29, 32]. Fig. 7 show our results.

The paths formed by the points in the order map for water collapse into a single line inside the structural anomaly region. This means that in the water case the order parameters are strongly coupled. For silica [10] and beryllium fluoride [17], also anomalous tetrahedral liquids, the orientational and translational order parameters are weakly coupled, since they develop a two-dimensional region in the order map of such liquids. For all λ considered in this work we have a silica- and beryllium fluoride-like behavior for the paths in the order map of our model. This means that the two scales potentials are hybrid models, in the sense that they can exhibit water-like hierarchy of

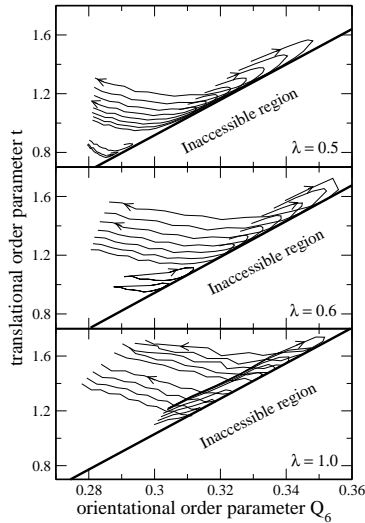


Fig. 7: Order map for the potential Eq. (1) with $\lambda = 0.5, 0.6$, and 1.0 . The arrows indicate the direction of increasing density for fixed temperatures. In the upper panel, the temperatures are (from top to bottom) $T^* = 0.08, \dots, 0.14, 0.15, 0.27, 0.33$, and 0.35 . In the middle panel, $T^* = 0.08, \dots, 0.13, 0.14, 0.18$, and 0.22 . Finally, in the lower panel, $T^* = 0.11, \dots, 0.14, 0.15, 0.18, 0.20$, and 0.22 .

anomalies [21, 32] but reproduce the order map of silica and beryllium fluoride instead of water. The understanding of the coupling mechanism of the order parameters is not clear in the literature, and we believe this could shade some light into important aspects of anomalous fluids.

Next, a remarkable feature of the order map shown in Fig. 7 is that the inaccessible region is virtually λ -independent. In all panels, the inaccessible region is bounded by a straight line given by $t = a_\lambda Q_6 + b_\lambda$, with $a_{0.5} = 12.05$, $a_{0.6} = 12.20$, and $a_{1.0} = 12.92$; $b_{0.5} = -2.70$, $b_{0.6} = -2.72$, and $b_{1.0} = -2.84$. The difference between the extreme values of a_λ and b_λ quantities is less than 7.5%. This means that the order in all λ -systems respond roughly constant upon compression. In this sense we are lead to believe that the two scales feature, which is present in all λ -cases considered here, is most important than energetic barriers differences between them towards the appearance of anomalies. Indeed, it was shown that structure and water-like anomalies can be linked by means of the excess entropy [44], stressing the importance of the role played by structural parameters into the understanding of the water-like anomalies.

In resume, the three anomalous regions respond differently to the change in the potential. The diffusion anomalous region shrinks in the pressure temperature phase-diagram and disappears in $T^* < 0.08$ for $\lambda = 0.65$ (not shown); the density anomalous region shrinks in pressure and reduces to a small region in $\lambda = 1.0$; the structural anomalous region also shrinks in pressure but it is still in the stable region of the pressure-temperature phase-diagram for $\lambda = 1.0$. The order map analysis show that

the inaccessible region in the $t - Q_6$ plane is virtually independent of λ and the order parameters are uncoupled, differently of water but similar to silica and beryllium fluoride.

Conclusions. – In this paper we have shown that two scales effective potentials always reproduce water-like anomalies. In this sense, any liquid material in which this kind of effective interaction is present is able to be an anomalous liquid. In some cases the anomalous regions are located in the pressure-temperature phase-diagram inside the region where the solid phase is the most stable, being inaccessible either with experiments or with equilibrium simulations.

In water the two scales distances – two energetic-competing preferable distances – clearly arise from the formation and breaking of hydrogen bonds. In other anomalous liquids this process come from different competing interactions but the *effective* final interparticle potential must be a two scales potential.

We believe that the knowledge of this mechanism can be of great interest for industries. The domain of this mechanism could lead to the development of new materials – polymers, for example – in which some anomalous properties could be used in the manufacture of substances close to its supercooled region. A polymer in which its molecules diffuses faster upon compression is an example of a possible application of these findings.

REFERENCES

- [1] WALER R., *Essays of natural experiments* (Johnson Reprint, New York) 1964.
- [2] ANGELL C. A., FINCH E. D. and BACH P., *J. Chem. Phys.*, **65** (1976) 3063.
- [3] PRIELMEIER F. X., LANG E. W., SPEEDY R. J. and LÜDEMANN H.-D., *Phys. Rev. Lett.*, **59** (1987) 1128.
- [4] ERRINGTON J. R. and DEBENEDETTI P. G., *Nature (London)*, **409** (2001) 318.
- [5] NETZ P. A., STARR F. W., STANLEY H. E. and BARBOSA M. C., *J. Chem. Phys.*, **115** (2001) 344.
- [6] THURN H. and RUSKA J., *J. Non-Cryst. Solids*, **22** (1976) 331.
- [7] SAUER G. E. and BORST L. B., *Science*, **158** (1967) 1567.
- [8] KENNEDY S. J. and WHEELER J. C., *J. Chem. Phys.*, **78** (1983) 1523.
- [9] TSUCHIYA T., *J. Phys. Soc. Jpn.*, **60** (1991) 227.
- [10] SHELL M. S., DEBENEDETTI P. G. and PANAGIOTOPOULOS A. Z., *Phys. Rev. E*, **66** (2002) 011202.
- [11] SASTRY S. and ANGELL C. A., *Nature Mater.*, **2** (2003) 739.
- [12] AGARWAL M., SHARMA R. and CHAKRAVARTY C., *J. Chem. Phys.*, **127** (2007) 164502.
- [13] ANGELL A., CHEESEMAN P. A. and TAMADDON S., *Science*, **218** (1982) 885.
- [14] TSUNEYUKI S. and MATSUI Y., *Phys. Rev. Lett.*, **74** (1995) 3197.
- [15] SHARMA R., CHAKRABORTY S. N. and CHAKRAVARTY C., *J. Chem. Phys.*, **125** (2006) 204501.
- [16] MORISHITA T., *Phys. Rev. E*, **72** (2005) 021201.
- [17] AGARWAL M. and CHAKRAVARTY C., *J. Phys. Chem. B*, **111** (2007) 13294.
- [18] CHAPLIN M., *Sixty-three anomalies of water* <http://www.lsbu.ac.uk/water/anmlies.html> (Sep. 2006).
- [19] HEAD-GORDON T. and STILLINGER F. H., *J. Chem. Phys.*, **98** (1993) 3313.
- [20] DE OLIVEIRA A. B., NETZ P. A., COLLA T. and BARBOSA M. C., *J. Chem. Phys.*, **124** (2006) 084505.
- [21] DE OLIVEIRA A. B., NETZ P. A., COLLA T. and BARBOSA M. C., *J. Chem. Phys.*, **125** (2006) 124503.
- [22] DE OLIVEIRA A. B., BARBOSA M. C. and NETZ P. A., *Physica A*, **386** (2007) 744.
- [23] MITTAL J., ERRINGTON J. R. and TRUSKETT T. M., *J. Chem. Phys.*, **125** (2006) 076102.
- [24] GIBSON H. M. and WILDING N. B., *Phys. Rev. E*, **73** (2006) 061507.
- [25] CAMP P., *Phys. Rev. E*, **71** (2005) 031507.
- [26] JAGLA E. A., *J. Chem. Phys.*, **111** (1999) 8980.
- [27] DE OLIVEIRA A. B., FRANZESE G., NETZ P. A. and BARBOSA M. C., *J. Chem. Phys.*, **128** (2008) 064901.
- [28] XU L., BULDYREV S., ANGELL C. A. and STANLEY H. E., *Phys. Rev. E*, **74** (2006) 031108.
- [29] YAN Z., BULDYREV S. V., GIOVAMBATTISTA N. and STANLEY H. E., *Phys. Rev. Lett.*, **95** (2005) 130604.
- [30] FOMIN D. Y., FRENKEL D., GRIBOVA N. V. and RYZHOV V. N., *J. Chem. Phys.*, **129** (2008) 064512.
- [31] FRANZESE G., *J. Mol. Liq.*, **136** (2007) 267.
- [32] YAN Z., BULDYREV S. V., GIOVAMBATTISTA N., DEBENEDETTI P. G. and STANLEY H. E., *Phys. Rev. E*, **73** (2006) 051204.
- [33] KREKELBERG W. P., MITTAL J., GANESAN V. and TRUSKETT T. M., *Phys. Rev. E*, **77** (2008) 041201.
- [34] YAN Z. Y., BULDYREV S. V., KUMAR P., GIOVAMBATTISTA N. and STANLEY H. E., *Phys. Rev. E*, **77** (2008) 042201.
- [35] BULDYREV S. V., KUMAR P., DEBENEDETTI P. G., ROSSKY P. J. and STANLEY H. E., *Proc. Natl. Acad. Sci. U.S.A.*, **104** (2007) 20177.
- [36] DE OLIVEIRA A. B., NETZ P. A. and BARBOSA M. C., *Euro. Phys. J. B*, **64** (2008) 481.
- [37] KUMAR P., BULDYREV S. V., SCIORTINO F., ZACCARELLI E. and STANLEY H. E., *Phys. Rev. E*, **72** (2005) 021501.
- [38] ALDER B. J. and WAINWRIGHT T. E., *J. Chem. Phys.*, **31** (1959) 459.
- [39] HAILE J. M., *Molecular Dynamics Simulation* 1st Edition (Wiley-Interscience, New York) 1997.
- [40] STEINHARDT P. J., NELSON D. R. and RONCHETTI M., *Phys. Rev. B*, **28** (1983) 784.
- [41] NETZ P. A., BULDYREV S., BARBOSA M. C. and STANLEY H. E., *Physical Review E*, **73** (2006) 061504.
- [42] SZORTYKA M. M. and BARBOSA M. C., *Physica A*, **380** (2007) 27.
- [43] GIRARDI M., SZORTYKA M. and BARBOSA M. C., *Physica A*, **386** (2007) 692.
- [44] ERRINGTON J. R., TRUSKETT T. M. and MITTAL J., *J. Chem. Phys.*, **125** (2006) 244502.